SCIENCE CHINA
Earth Sciences

• RESEARCH PAPER •

June 2015 Vol.58 No.6: 996–1004
doi: 10.1007/s11430-014-5032-z

The numerical simulation of caesium-137 transportation in ocean and the assessment of its radioactive impacts after Fukushima NPP release

GUAN Yue, SHEN ShiFei* & HUANG Hong

Institute of Public Safety Research, Department of Engineering Physics, Tsinghua University, Beijing 100084, China

Received July 14, 2014; accepted October 23, 2014; published online April 17, 2015

After the damage of Fukushima Daiichi Nuclear Power Plant, a great number of radioactive materials were released into the Pacific Ocean. Therefore, it is necessary to research on the temporal and spatial distribution of these radionuclides. We use Princeton Ocean Model to simulate the circulation of the coast water of Fukushima NPP and obtain the concentration of caesium-137 by solving the diffusion equations. We employ the Monte Carlo N-particle (MCNP) code to assess the external doses caused by these contaminated sea water. To improve the efficiency and effectiveness of volume source in MCNP code, we establish a transformation method between spot source and volume source, and determine an appropriate range of volume source. Finally, we calculate the absorbed doses of every organ/tissue and the effective dose of a human body.

numerical simulation, POM, caesium-137, MCNP, absorbed dose, effective dose

Citation: Guan Y, Shen S F, Huang H. 2015. The numerical simulation of caesium-137 transportation in ocean and the assessment of its radioactive impacts after Fukushima NPP release. Science China: Earth Sciences, 58: 996−1004, doi: 10.1007/s11430-014-5032-z

An unexpected *M*9.0 earthquake occurred in Japan on March 11, 2011. Then, the cooling system of reactors in the Fukushima Daiichi Nuclear Power Plant was damaged by the subsequent tremendous tsunami. Tokyo Electric Power Company (TEPCO) used seawater to cool the reactor cores, which caused the contaminated water released into the Pacific Ocean.

Many Oceanic General Circulation Models (OGCM) have been developed to simulate the dispersion processes of tracers in oceans in recent decades, such as the Miami Isopycnic Coordinate Ocean Model (MICOM) (Orre et al., 2010), North Atlantic-Arctic Ocean Sea Ice Model (NAOSIM) (Karcher et al., 2004), NCAR Climate System Model Ocean Model (NCOM) (Aoyama et al., 2008), the unstructured grid Finite Volume Coastal Ocean Model (FVCOM) (Chen et al., 2006), Hybrid Coordinate Ocean Model (HYCOM) (Bleck et al., 2002; Wallcraft et al., 2003) and so forth. Several groups have studied numerical simulations of radionuclides from the Fukushima NPP by the above mentioned models, such as Tsumune et al. (2012) who employed ROMS to simulate the circulation of the Northeast Pacific Ocean and assess the concentration of radionuclides; Behrens et al. (2012) estimated the long-term dispersion after Fukushima nuclear crisis; Qiao et al. (2011) estimated the spread of nuclear radiation and predicted the time to spread to Europe and America. Note that most of them focused merely on the dispersion of contaminants, while the radioactive impacts of the contaminated water are less studied.

In this article, we employ the Princeton Ocean Model (POM) to simulate the circulation of the coast water of the Fukushima NPP. On the basis of the simulation result from POM, such as 3-dimensional velocities, water level, tem-

*Corresponding author (email: shensf@mail.tsinghua.edu.cn)

perature, and other physical quantities, we solve the diffusion equations of passive tracer and obtain the concentration of caesium-137 released from the Fukushima Daiichi Nuclear Power Plant. Furthermore, we apply MCNP to assess the absorbed doses to human organs or tissues and evaluate the effective dose obtained from the contaminated sea water.

1 Numerical simulation of oceanic circulation and ^{137}Cs transportation

1.1 Model configuration and input data

We employed the Princeton Ocean Model (Blumberg et al., 1987) to simulate the circulation of the coast water of the Fukushima NPP and the dispersion of ^{137}Cs. POM is a three-dimensional ocean circulation model, which employs sigma coordinate in the vertical coordinate and curvilinear horizontal orthogonal grids to adapt to complex topography. Due to its simplicity and maturity, POM (Mellor, 2004) has become a very popular OGCM. It has been used successfully to simulate the circulation of oceans and the transportation of tracers, such as the North Atlantic Ocean (Ezer et al., 2000), the Grand Banks of Newfoundland (Chen et al., 2010) and so on.

The model domain in this research covered the coast water of east of Fukushima (140.5°–142.5°E and 35.75°–38.75°N). The horizontal grid configuration is 101 meshes in zonal direction and 151 meshes in the meridional direction, whose resolution is around 2 km×2 km. There are 8 layers in vertical direction. The time step for 3-D equations is 60 s and the barotropic mode is executed 20 times in each 3-D step. Surface elevation at open lateral boundary is set as clamped, other variables are set to radiation boundary condition. POM employs "leap frog" difference scheme. The horizontal time differencing is explicit whereas the vertical differencing is implicit. We choose Smolarkiewicz iterative upstream scheme as advection scheme and choose POM's default settings for other schemes.

The topography data of this study are from ETOPO2 data structure which is supported by National Geophysical Data Center. Coverage of ETOPO2v2 is −90° to +90° in latitude, and −180° to +180° in longitude. The resolution of this topography is 2′. The air-sea exchange processes are indispensable for understanding and predicting oceanic circulation. This model is forced at the sea surface by wind stress, whose values are acquired from the Cross-Calibrated Multi-Platform Ocean Surface Wind Velocity (CCMP). The surface stress tensors used in this research are calculated from the CCMP wind field through the following equation (Wu, 1982):

$$\tau = \rho_a r_a \vec{W} |\vec{W}|, \tag{1}$$

where τ is the wind stress acting on the sea surface (N); ρ_a represents the density of air (kg m^{-3}), r_a = (0.8+0.065 × $|\vec{W}|$)×10^{-3} is the wind-stress coefficient; $|\vec{W}|$ is the speed measured at 10 m above the mean sea surface (m s^{-1}).

Tidal current plays an important role in the flow field of near shore zone and, hence, has a great impact on the transportation of tracers in this area. The sea surface elevations of open boundaries are predicted by the tidal harmonic analysis and import to the model.

$$\eta(t) = \sum_i f_i H_i \cos[\sigma_i t + (V_0 + u)_i], \tag{2}$$

where η represents the sea surface elevation (m), σ_i is the frequency of tidal constituent I (degree h^{-1}), H_i represents the magnitude of tidal constituent I (m), f_i is the tidal factor, and $(V_0+u)_i$ is initial phase (degree). The tidal constants are acquired from Tide Model Driver TPXO7.1 (Egbert et al., 2002). Four major tidal constituents are imported in this model, namely, M2, S2, K1, and O1 tidal constituents. The amplitudes of other constituents are relatively small and negligible.

Cs is treated as a passive tracer which advects and diffuses in ocean, and the concentration in seawater decays with a half-life of 30.17 years. To calculate the dispersion process of radioactive pollutant, we use Euler method:

$$\frac{\partial DC}{\partial t} + \frac{\partial UDC}{\partial x} + \frac{\partial VDC}{\partial y} + \frac{\partial \omega C}{\partial \sigma} = \frac{\partial}{\partial \sigma}\left(\frac{K_H}{D}\frac{\partial C}{\partial \sigma}\right) + DC_0 + \frac{\partial}{\partial x}\left(A_H D \frac{\partial C}{\partial x}\right) + \frac{\partial}{\partial y}\left(A_H D \frac{\partial C}{\partial y}\right) - \lambda DC, \tag{3}$$

where C is the concentration of pollutant, C_0 is the source term, and λ is the decay coefficient. Other symbols are consistent with POM's equations.

1.2 Source term

Plenty of radioactive materials were released into the Pacific Ocean along with the water coolant after the damage of the Fukushima Daiichi Nuclear Power Plant. Among these nuclides, the caesium-137 is the most important contaminant because of its long half-life period ($T_{1/2}$=30.17 years) and huge release amount (assessed to about 4 PBq for direct effluent release (Kawamura et al., 2011; Nakano et al., 2012), 1 PBq=10^{15} Bq). To monitor the concentration of nuclides in seawater, TEPCO (owner of the Fukushima Daiichi NPP) sets up several sites to observe radioactivity, such as the southern discharge canal of the Fukushima Daiichi Nuclear Power Plant (1F), northern discharge canal of the Fukushima Daini Nuclear Power Plant (2F, approximately 10 km from 1F) and 2F Iwasawa Coast (approximately 16 km from 1F). Figure 1 shows the observed spots used in this article.

The information of release rate of caesium-137 from the

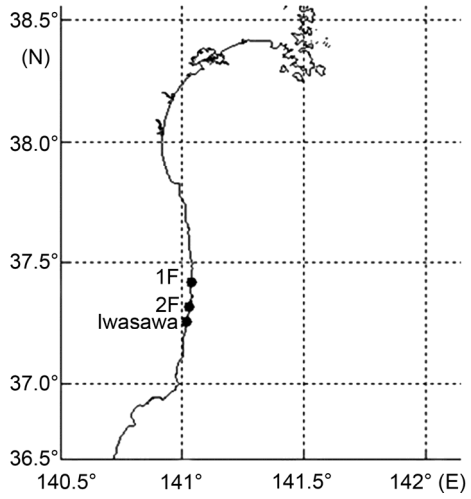

Figure 1 Observed sites of Fukushima coast.

Fukushima Daiichi Nuclear Power Plant is very difficult to estimate. The source term of this model is based on the assumption of Tsumune et al. (2012) who estimated the ^{137}Cs release rate by utilizing the TEPCO press releases to the public and their own numerical simulations. The source term is imported as a direct release of radioactive water to the Pacific Ocean. The indirect path, namely the deposition from the atmosphere is not taken into consideration.

In Tsumune's assumption, the direct release started on 26 March. However, in TEPCO's observation, they have detected Cs-137 nuclides at discharge canal of 1F since 21 March. On the basis of the assumption of Tsumune and TEPCO's data, we apply a release scenario that the direct leakage started on 21 March, 2011, ten days after the Fukushima earthquake; the release rate of caesium-137 was 2.20×10^{14} Bq d^{-1} (2.55×10^{9} Bq s^{-1}) from 21 March to 6 April. The observed concentration from TEPCO decreased exponentially since 6 April and then remained constant after 26 April, 2011. Therefore, we applied the exponentially decreased release rate from 6 April to 26 April. And the release rate from 26 April to 31 May is set to constant 2.20×10^{12} Bq d^{-1} (1% of the initial release rate). This scenario is almost the same with Tsumune's assumption except for the direct release from 21 March to 25 March. The assumed total release amount is 4.4 PBq which is in agreement with other researchers' assumption (Nakano et al., 2012; Kawamura et al., 2011).

1.3 Simulation results

Figures 2–4 show the comparisons of sea surface ^{137}Cs concentration between the observed data pressed by TEPCO and the simulation in this model at three different locations respectively. The blue lines represent the simulation results computed by POM and our embedded diffusion subroutine for passive tracers, whereas the red squares are the observed sea surface concentration provided by TEPCO. The locations of these three spots are plotted in Figure 1.

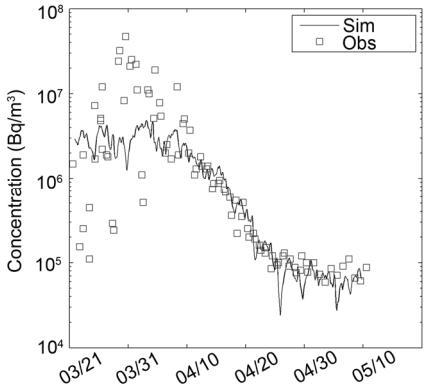

Figure 2 Comparison of observation data and simulation result at discharge canal of 1F (sea surface concentration of ^{137}Cs).

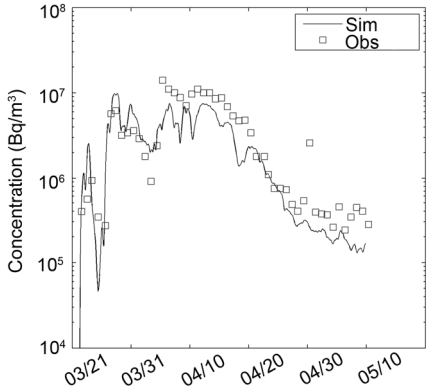

Figure 3 Comparison of observation data and simulation result at discharge canal of 2F (sea surface concentration of ^{137}Cs).

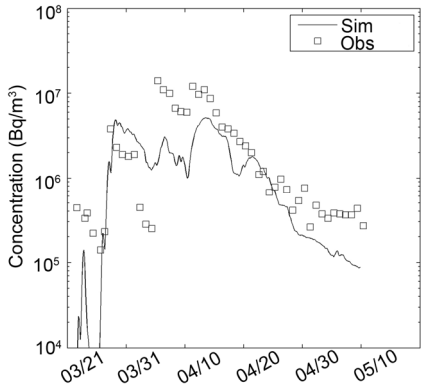

Figure 4 Comparison of observation data and simulation result at 2F Iwasawa Coast (sea surface concentration of ^{137}Cs).

As shown in Figure 2, the simulated sea surface concentration of caesium-137 was in a reasonable agreement with the observed data from TEPCO in the southern discharge canal of the Fukushima Daiichi Nuclear Power Plant. At the beginning of release, the observed concentration from TEPCO oscillates greatly, which may be caused by a continuously changing release rate. The simulation result has

much less oscillation due to the constant release rate assumption in the early discharge. Observed concentration decreases exponentially since 6 April or so, which is reproduced by the model pretty well. From around 26 April, both the observed data and the simulation concentration tend to remain a relatively constant value.

At the discharge canal of 2F NPP, as depicted in Figure 3, the concentration peaks around 24 March, 28 March, 5 April and 11 April are consistently reproduced by the simulation results. After the exponential decrease, the simulation concentrations begin to maintain a constant around 3×10^4 Bq m^{-3}, which is the same as the observed data from TEPCO.

As for the Iwasawa Shore observation spot, the observation concentration peaks in 24 March, 28 March, 5 April and 11 April are reproduced. However, the simulation concentrations in these days are underestimated slightly. One possible reason for this underestimation is that the grid we applied is not fine enough to represent the variations at shore monitoring spots. This phenomenon is more obvious in Iwasawa shore than in the Fukushima Daini NPP, because of the different distance to source.

The concentration increases if the current velocity is low, while it decreases if the current velocity is high, which causes the peaks and troughs in a constant release rate in early leakage.

To validate the simulation in off-shore region, we compare the POM output with the observation data from TEPCO (http://www.tepco.co.jp/en/nu/fukushima-np/f1/index2-e. html) and MEXT (Ministry of Education, Culture, Sports, Science and Technology, Japan) (http://radioactivity.nsr.go.jp/ja/list/273/list-1.html). The comparison result is depicted in Figure 5.

The observation data from MEXT are very sparse in time dimension. Therefore, in order to decrease the random error from observation, we apply the time average concentration to compare with POM result. The simulated concentration is depicted in Figure 5, and the observation data were scattered as many triangles. The filled colors of these triangles represent the observed concentration. In the period from 28 March to 3 April (around 1 week after the discharge began), the concentration is underestimated for off-shore region. One reason for the underestimation is the atmosphere deposition. The dispersion in atmosphere is much faster than in ocean. Therefore, the Cs-137 from direct effluent release did not spread to the observation places while the nuclides deposited from atmosphere could be detected there. In the period from 18 April to 24 April (around 1 month after the discharge started), the simulation result is in a reasonable agreement with the observation, which demonstrates the validation of the simulation. A detailed analysis and comparison of the model result is discussed elsewhere.

Figure 6 shows the temporal and spatial distribution of sea surface caesium-137 concentration on 22 March, 1 April, 11 April, 21 April and 1 May. ^{137}Cs discharged from the Fukushima Daiichi NPP was dispersed southward along the coast line and spread to the Northwest Pacific Ocean. A mesoscale eddy is simulated by the POM code, which reproduces the findings of Tsumune et al. (2012), who employed another model (ROMS) as the oceanic general circulation model. As shown in Figure 6, at the beginning of release, the ^{137}Cs concentration of sea surface peaked to above 10^6 Bq m^{-3} in the vicinity of 1F, and decreased to 10^4 Bq m^{-3} in May with the diffusion and spread in the open ocean.

2 Radioactive doses

The internal dose is mainly from ingestion of seafood caught from the sea surface, such as fish, crustaceans, cephalopods, shellfish and seaweed. The external dose is caused by marine operations. The internal dose was calculated by many previous researches (Maderich et al., 2013; Nakano et al., 2012; Nielsen et al., 1999), whereas the external dose was less studied (Buesseler et al., 2012). However, it is necessary to study the external radiation exposure to estimate the total risk of radio nuclides in ocean. And it could provide the requisite support to the risk warning for the rescue operations and emergency personnel in the nearby waters. In this article, we assess the external dose from hypothetical floating in near shore ocean surface area for a person (e.g. a swimmer or snorkeller).

2.1 MCNP

The Monte Carlo N-Particle Transport Code (MCNP) is developed by the Los Alamos National Laboratory (X-5 Monte Carlo Team, 2003). As a popular software package used for radioactive particle transport simulation and modeling MCNP is used successfully to calculate the absorbed dose in practical radiotherapy (Lazarine, 2006). In this study, the MCNP code (version 5) was employed to assess the external dose caused by the radionuclides released from the Fukushima Nuclear Power Plant.

The calculation process of MCNP in this application could be summarized as follows:

(1) Set up a human model which includes the definition of different organ and tissue with their properties such as density, volume, constituent elements and so forth.

(2) Set up a volume source surrounding the human model. The property of the volume is consistent with sea water and the radioactive source is set to Cs-137.

(3) MCNP generates a source particle (for instance, γ ray) and tracks its trace until it vanished or escaped outside the research domain. If the source particle stimulates some secondary particles (photons or electrons), MCNP will track them too and record the accumulated energy of each organ/tissue until all particles vanished or escaped.

(4) MCNP repeats the third step over and over again (more than 50 million times in this research) and averages

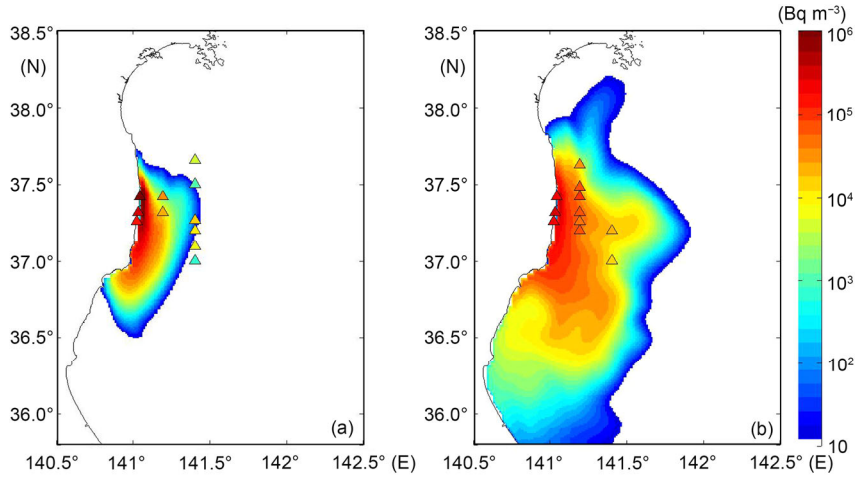

Figure 5 Simulated sea surface caesium-137 average concentration from 28 March to 3 April (a) and average concentration from 18 April to 24 April (b).

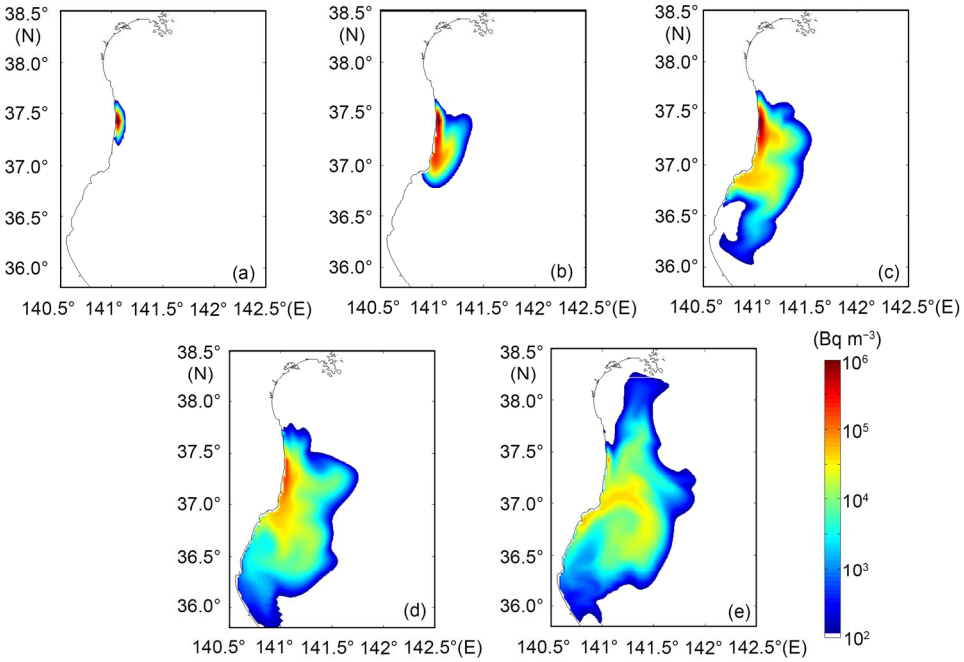

Figure 6 Simulated sea surface caesium-137 concentration on 22 March (a), 1 April (b), 11 April (c), 21 April (d) and 1 May (e).

the absorbed energy of every organ to one source particle. Then, we acquire a credible absorbed energy rate with a little uncertainty.

2.2 Volume source scale

Caesium-137 mainly emits a 511.6 keV β-ray and a 661.7 keV γ-ray during its decay. Because the range of β-ray is pretty limited in water, only the γ-ray was taken into consideration. Volume source was employed in MCNP to represent the γ-ray emitted from ^{137}Cs in sea water, and person tally is located in the center of the volume source to record the absorbed dose. Based on the Monte Carlo method, MCNP will generate a great number of particles and simulate and record the entire trace of every particle. Every single particle will be generated randomly in some position within the volume source and be shot to a random angle. Therefore, if the volume source scale is dispensably large, many particles born far from the human tally have few opportunities to have an impact on the tally, which leads to a waste of computing resource and time. Hence, it is necessary to find an appropriate range to make sure that the absorbed dose contributed from ^{137}Cs out of the range is negligible compared with the dose from the inside.

To determine an appropriate volume source scale, we need to establish a transformation approach between spot source and volume source. We use detection efficiency to represent the validation of a transformation method. Detec-

tion efficiency means the detection possibility when a particle is generated randomly in the source. If a huge number of particles are born randomly, based on the Monte Carlo theory, the detection possibility will tend to be a constant, namely the detection efficiency. There are many factors influencing detection efficiency from a spot source: the distance between the source and detector, the kind and density of surrounding media, the shape of detector, etc. Two major factors influence the efficiency greatly. First, the intensity of γ-ray decreases exponentially with the distance photons transport based on the total cross section Σ of the media. So, there is a $e^{-\Sigma r}$ term in the spot source detection efficiency formula (r is the distance between spot source and detector). Second, the efficiency is proportional to the volume angel spanned by detector, namely $A/4\pi r^2$, where A is cross-sectional area. Therefore, the detection efficiency of spot source can be expressed as

$$\varepsilon = C\frac{A}{4\pi r^2}e^{-\Sigma r}, \tag{4}$$

where C is a constant associated with the detector's shape and other factors. Take a constant G and let $G=CA/4\pi$. Eq. (4) converts to

$$\varepsilon = \frac{G}{r^2}e^{-\Sigma r}. \tag{5}$$

Then, the detection efficiency of a volume source could be represented by many random located spot sources in the volume source. For instance, the detection efficiency of a sphere volume source could be calculated by

$$\varepsilon_{\text{sphere}} = \frac{1}{V}\int_{r_0}^{R} 4\pi r^2 \varepsilon_{\text{spot}}\,\mathrm{d}r = \frac{1}{\frac{4\pi}{3}R^3}\int_{r_0}^{R} 4\pi r^2 \frac{G}{r^2}e^{-\Sigma r}\mathrm{d}r$$
$$= \frac{3G}{R^3}\int_{r_0}^{R} e^{-\Sigma r}\mathrm{d}r = \frac{3G}{R^3\sum}(e^{-\Sigma r_0} - e^{-\Sigma R}), \tag{6}$$

where V represents the volume of sphere source, r_0 is the scale of the sphere detector located in the center of the source, R is the radium of the sphere source.

We apply a series of simulations by MCNP to confirm the above theory. We locate a hypothetical sphere NaI scintillation detector (radium is 5 cm) in the center of a huge volume of sea water, and placed a spot γ-ray source (energy=0.6617 Mev) in different distances. Tally F8 is employed to record the counts of full-energy rays. The calculation results are shown in Figure 7.

Crosses in Figure 7 represent the MCNP calculation result. The error bars show the statistical fluctuation of detection efficiencies of each spot source. The curve is the fitting curve based on eq. (5). As shown in Figure 7, the detection efficiency decreases very quickly with the distance increasing. The fitting curve is in a good agreement with the MCNP result except for the near detector positions. The

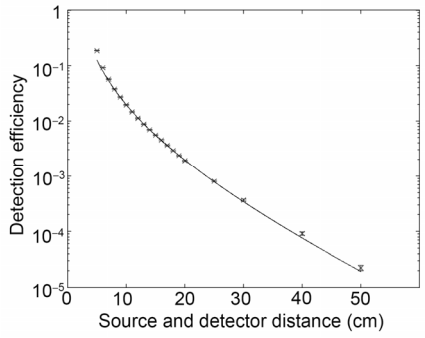

Figure 7 The curve of detection efficiency and distance.

normalized volume angel spanned by sphere-shape detector could be calculated through the following equation:

$$\alpha = \frac{1}{2}\left(1 - \sqrt{1 - \left(\frac{r_0}{r}\right)^2}\right), \tag{7}$$

where r_0 is the radium of the sphere detector, r represents the distance between source and detector. In the place far from the source region $r_0 \ll r$, eq. (7) converts to

$$\alpha = \frac{1}{2}\left(1 - \sqrt{1 - \left(\frac{r_0}{r}\right)^2}\right) \approx \frac{1}{2}\left[1 - \left(1 - \frac{1}{2}\frac{r_0^2}{r^2}\right)\right]$$
$$= \frac{r_0^2}{4r^2} = \frac{\pi r_0^2}{4\pi r^2} \propto \frac{1}{r^2}, \tag{8}$$

Eq. (8) means the volume angle of the spot source far from the detector can be calculated through dividing the projected area of sphere detector (πr_0^2) by surface area of distance sphere ($4\pi r^2$). However, in the vicinity of detector, volume angel is not proportional to $1/r^2$, which causes fitting curve underestimating the detection efficiency of near-detector sources, as shown in Figure 7. However, the correlation coefficient R^2 is 0.99988 for the spot sources farther than 10 cm, which indicates the great agreement with the MCNP calculation results of these sources.

Furthermore, we apply a volume source simulation by MCNP. The efficiency of a sphere sea water source whose radium is 100 cm is calculated. The result from MCNP is 1.0448×10^{-4} and the statistical error is 1.68%. The efficiency calculated by eq. (6) is 1.0271×10^{-4}. The relative error between MCNP result and eq. (6) result is very small (around 1.69%), which is comparable with the statistical error (1.68%) of MCNP calculation. Therefore, this is an effective transformation method between spot source and volume source. On the basis of above theories and eq. (6), we try to choose an appropriate range to ensure that the detection efficiency for the outside γ-ray is negligible.

Table 1 shows the detection efficiencies of different volume source range. We can conclude that the detection efficiency is contributed mainly by the near detector γ-rays.

Table 1 Relationship between volume source range and detection efficiency

Range (cm)	Detection Efficiency calculated by eq. (6)		Outside/inside
	γ-ray inside the range	γ-ray outside the range	
20	7.6099×10^{-5}	2.6632×10^{-5}	0.349965376
40	9.8329×10^{-5}	4.4022×10^{-6}	0.044770644
60	1.0200×10^{-4}	7.2768×10^{-7}	0.007133942
80	1.0261×10^{-4}	1.2029×10^{-7}	0.001172252
100	1.0271×10^{-4}	1.9883×10^{-8}	0.000193583

The photons emitted in far-from-detector region are hardly detected, because of the shielding of sea water. Actually, MCNP will be very time consuming to obtain small enough statistical error, if the detection efficiency is too low. This is the reason why we cannot obtain the detection efficiencies of far-from-detector spot sources directly and have to calculate them by eq. (5). On the basis of the calculation in Table 1, we choose 80 cm to be the range of volume source, which makes that the detection efficiency contributed from γ-rays out of the range is only 0.1% of the contribution from the inside.

2.3 Absorbed dose and effective dose

Utilizing MCNP code, we calculate absorbed doses for different organs or tissues which are defined in the ORNL MIRD phantom developed by scholars at Hanyang University (Lazarine, 2006). The human model floats in contaminated sea water. For the source term, we apply a volume source whose size is 80 cm larger than the human cell defined in every 3-dimensional direction except in the direction of face. 661.6 keV γ-ray is generated randomly in the volume source and is shot to a random angel. The organ tallies include: ovaries/testes, bones, intestines, lungs, stomach, bladder wall, kidney, liver, brain, adrenals, thyroid, pancreas, spleen, thymus, uterus, esophagus, skins and other organs and tissues. The geometry specification in this model is plotted in Figure 8. The volume sea water source (green in Figure 8) is almost a semi-ellipsoid, which is not wholly drawn.

The materials in this model are also described in the ORNL MIRD input deck. The results of MCNP are summarized in Table 2. Because the absorbed doses are relative with the concentration of radionuclides and time, we import UOC (unit of concentration) into the calculation result. We define 1 UOC = 1 Bq L^{-1} = 1 decay s^{-1} L^{-1}. The method to calculate absorbed energy is as follows: MCNP randomly generates a lot of radioactive particles (which are more than 50 million in this case) and calculate the absorbed energy of each organ/tissue. Then it averages the energy to each particle, and the numbers are shown in the 4th column in Table 2.

As shown in Table 2, the absorbed doses of every organ/tissue are almost the same. The highest absorbed doses are in skins and bones, above 5.5×10^{-14} Gy UOC^{-1} s^{-1}. It is intelligible that the absorbed dose in skins is higher than other tissues because skins are adjacent to sea water source. It is needed to note that bones have higher density. Generally speaking, the higher the organ density, the higher the possibility of interaction between γ-ray and atoms. Therefore, the absorbed dose of bones is higher too. The lowest absorbed dose is from the "Bladder wall" tissue (around 3.1×10^{-14} Gy UOC^{-1} s^{-1}). Su et al. (2011) employed MCNP to calculate radiation doses of artificial radionuclides for 11 radiation reference species such as: shrimp, crab, cuttlefish and so forth. The absorbed doses of different species from Caesium-137 source ranges from 2.2×10^{-15} to 5×10^{-14} Gy UOC^{-1} s^{-1}, which is in good agreement with our results.

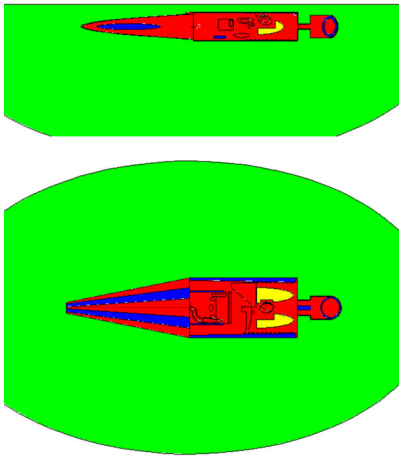

Figure 8 Geometry specification.

Effective dose is calculated by

$$E = \sum_{\mathrm{T}} (H_{\mathrm{T}} \times w_{\mathrm{T}}), \tag{9}$$

where H_{T} is the absorbed dose of organ/tissue T, w_{T} is the tissue weighting factor of organ/tissue T. In this model, the effective dose is around 5.5×10^{-14} Sv UOC^{-1} s^{-1}=2.0×10^{-10} Sv UOC^{-1} h^{-1}. Because the concentration of sea surface water around the Fukushima NPP is very high (10^5–10^7 Bq m^{-3} or 10^2–10^4 UOC for around discharge canal of 1F, and 10^4–10^6 Bq m^{-3} or 10^1–10^3 UOC for around discharge canal of 2F and Iwasawa shore, as shown in Figures 2–4), the effective dose can peak to 10^{-7}–10^{-6} Sv h^{-1} in near coast regions.

The hourly absorbed doses of sea surface from caesium-137 in 22 March, 6 April, 21 April and 6 May are shown in Figure 9. The ^{137}Cs advected southward along the coast and raised the surface absorbed doses near shore. Though the absorbed doses are extremely high in early release, they decrease very fast with the ocean circulation and dispersion. From May, 2011, most of hourly absorbed doses have been under 10^{-8} Sv h^{-1}, which is only 1% of the early doses near the Fukushima Daiichi NPP.

Nakano et al. (2012) assessed the effective dose commitment with intake of marine products found at the

Table 2 Absorbed dose of organs/tissues

Organ/tissue	Volume[a] (cm^3)	Density[a] ($g\ cm^{-3}$)	Absorbed energy (10^{-3} Mev $UOC^{-1}\ s^{-1}$)	Statistical error	Absorbed dose (10^{-14} Gy $UOC^{-1}\ s^{-1}$)	Tissue weighting factor[b]
Ovaries	8.38	1.04	1.728	0.1227	3.176	0.2
Testes	37.6	1.04	9.279	0.0641	3.802	0.2
Bones	7218	1.40	3495	0.0035	5.541	0.04[c]
Intestines	1793	1.04	397.4	0.01	3.415	0.12
Lungs	3370	0.296	285.8	0.0111	4.590	0.12
Stomach	402	1.04	90.38	0.0208	3.464	0.12
Bladder wall	45.7	1.04	9.267	0.0561	3.124	0.05
Kidney	288	1.04	87.39	0.0202	4.674	0.05
Liver	1830	1.04	474.8	0.0096	3.997	0.05
Brain	1370	1.04	491.1	0.0096	5.523	0.05
Adrenals	15.7	1.04	4.415	0.0814	4.332	0.05
Thyroid	19.9	1.04	6.566	0.0733	5.083	0.05
Pancreas	90.7	1.04	20.73	0.0399	3.521	0.05
Spleen	176	1.04	51.66	0.0267	4.522	0.05
Thymus	20.1	1.04	4.217	0.0909	3.232	0.05
Uterus	76	1.04	17.85	0.0439	3.619	0.05
Esophagus	44.7	1.04	11.60	0.0512	3.998	0.05
Skins	2968	1.04	1092	0.0056	5.670	0.01
Others	70480	1.04	15550	0.0025	3.398	0.05

a) The density and volume of each organ are exacted from the ORNL MIRD phantom (Lazarine, 2006); b) the weighting factors are referred from Chen et al. (2009); c) the tissue weighting factor of bone marrow is 0.12; the factor of bone surface is 0.01. We employ that the bone marrow is composed of about one fourth bone. Therefore, we use 0.04 as the tissue weighting factor of bone.

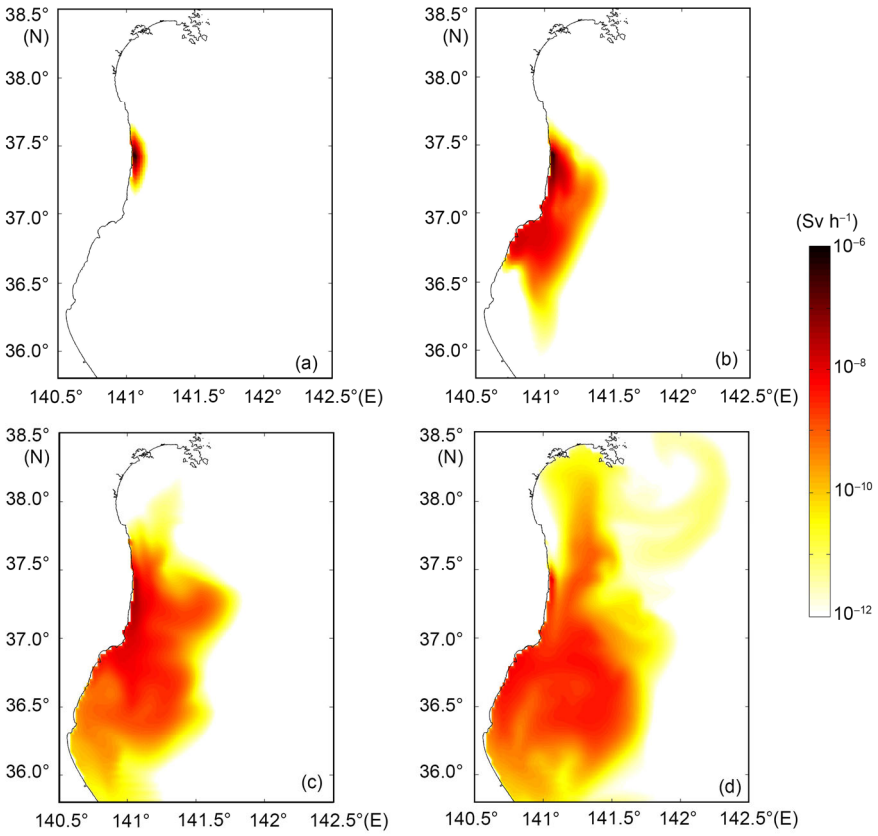

Figure 9 Simulation hourly absorbed doses of sea surface from caesium-137 in 22 March (a), 6 April (b), 21 April (c) and 6 May (d).

Northwest Pacific Ocean after the Fukushima NPP release is about 1.7×10^{-6} Sv yr^{-1}. Maderich et al. (2013) established that the individual dose rate for Fukushima, due to consumption of fishery products, is about 3.6×10^{-6} Sv yr^{-1}. Therefore, floating or swimming in the high concentration sea water for some hours will obtain the equal effective dose from intake marine products for a whole year. Buesseler et al. (2012) found the external dose to humans who immersed/swimming in 1000 Bq m^{-3} water is <0.01 μSv d^{-1}. Namely, the effective dose is $<4\times10^{-10}$ Sv UOC^{-1} h^{-1}, which is comparable with our result, 2.0×10^{-10} Sv UOC^{-1} h^{-1}.

3 Conclusion

The Princeton Ocean Model is used to simulate the circulation of coastal waters of the northwest Pacific Ocean after the release of the Fukushima Daiichi Nuclear Power Plant. On the basis of the source term assumption, we simulate the transportation processes of radioactive caesium-137, and obtain the concentration distribution. The simulated concentration of caesium-137 is in good agreement with the observed data pressed by TEPCO. The concentration is about 10^5–10^7 Bq m^{-3} in the near shore regions.

We use MCNP code to determine an appropriate range of volume source in calculating the absorbed doses of contaminated sea water. We establish a transformation method between spot source and volume source in sea water. The calculation result agrees with our theory, and we choose 80 cm to be the scale of volume source.

Finally, utilizing MCNP, we calculate the absorbed doses of every organ/tissue contributed from floating in a near shore region. The effective dose assessed from floating person tally in high concentration sea water for several hours can peak to 10^{-6} Sv, which is almost equal to the yearly effective dose commitment with intake of marine products found at the Northwest Pacific Ocean after the Fukushima NPP release.

This study was supported by the National Natural Science Foundation of China (Grant No. 71373140), the State Key Laboratory of NBC Protection for Civilian (Grant No. SKLNBC0308), and Tsinghua University Initiative Scientific Research Program (Grant Nos. 2012Z10137, 2012THZ0124). This article benefited from the comments and suggestions of three anonymous reviewers. We are grateful for their suggestions.

Aoyama M, Hirose K, Nemoto K, et al. 2008. Water masses labeled with global fallout 137Cs formed by subduction in the North Pacific. Geophys Res Lett, 35: L016041

Behrens E, Schwarzkopf F U, Lubbecke J F, et al. 2012. Model simulations on the long-term dispersal of Cs-137 released into the Pacific Ocean off Fukushima. Environ Res Lett, 7: 0340043

Bleck R, Halliwwell G, Wallcraft A, et al. 2002. Hybrid coordinate ocean model. User's Manual

Blumberg A F, Meller G L. 1987. A description of a three-dimensional coastal ocean circulation model. In: Heaps N, ed. Three-Dimensional Coastal Ocean Models. Am Geophys Union, 68: 1–16

Buesseler K O, Jayne S R, Fisher N S, et al. 2012. Fukushima-derived radionuclides in the ocean and biota off Japan. Proc Natl Acad Sci USA, 109: 5984–5988

Chen C, Beardsley R C, Cowles G. 2006. An unstructured grid, finite-volume coastal ocean model FVCOM. User's Manual

Chen J, Tang B, Ma J, et al. 2009. He Anquan Zonghe Zhishi Xiuding Ban (in Chinese). Beijing: China Environmental Science Press

Chen Z, Zhao L, Lee K. 2010. Environmental risk assessment of offshore produced water discharges using a hybrid fuzzy-stochastic modeling approach. Environ Model Softw, 25: 782–792

Egbert, G D, Erofeeva S Y. 2002. Efficient inverse modeling of barotropic ocean tides. J Atmos Ocean Technol, 19: 183–204

Ezer T, Mellor G L. 2000. Sensitivity studies with the North Atlantic sigma coordinate Princeton Ocean Model. Dyn Atmos Oceans, 32: 185–208

Karcher M J, Gerland S, Harms I H, et al. 2004. The dispersion of Tc-99 in the Nordic Seas and the Arctic Ocean: A comparison of model results observations. J Environ Radioact, 74: 185–198

Kawamura H, Kobayashi T, Furuno A, et al. 2011. Preliminary numerical experiments on oceanic dispersion of I-131 and Cs-137 discharged into the ocean because of the Fukushima Daiichi Nuclear Power Plant disaster. J Nucl Sci Technol, 48: 1349–1356

Lazarine A D. 2006. Medical physics calculations with MCNP: A primer. Doctoral Dissertation. Texas A&M University

Maderich V, Bezhenar R, Heling R, et al. 2014. Regional long-term model of radioactivity dispersion and fate in the Northwestern Pacific and adjacent seas-application to the Fukushima Daiichi accident. J Environ Radioact, 131: 4–18

Mellor, G L. 2004. User's Guide for a Three-dimensional Primitive Equation Numerical Ocean Model. New Jersey: Princeton University

Nakano M, Povinec P P. 2012. Long-term simulations of the Cs-137 dispersion from the Fukushima accident in the world ocean. J Environ Radioact, 111: 109–115

Nielsen S P, Bengtson P, Bojanowsky R, et al. 1999. The radiological exposure of man from radioactivity in the Baltic Sea. Sci Total Environ, 238: 133–141

Orre S, Smith J N, Alfimov V, et al. 2010. Simulating transport of 129I and idealized tracers in the northern North Atlantic Ocean. Environ Fluid Mech, 10: 213–233

Qiao F L, Wang G S, Zhao W, et al. 2011. Predicting the spread of nuclear radiation from the damaged Fukushima Nuclear Power Plant. Chin Sci Bull, 56: 1890–1896

Su J, Zeng Z, Yu W, et al. 2011. Monte Carlo calculation of artificial radionuclide radiation doses for aquatic organisms in the sea area around Daya Bay Nuclear Power Plant (in Chinese). J Oceanogr Taiwan Strait, 3: 301–309

Tsumune D, Tsubono T, Aoyama M, et al. 2012. Distribution of oceanic 137Cs from the Fukushima Daiichi nuclear power plant simulated numerically by a regional ocean model. J Environ Radioact, 111: 100–108

Wallcraft A, Carroll S N, Kelly K A, et al. 2003. Hybrid coordinate ocean model. User's Guide

Wu, J. 1982. Wind-stress coefficients over sea-surface from breeze to hurricane. J Geophys Res Oceans Atmos, 87: 9704–9706

X-5 Monte Carlo Team. 2003. MCNP—A general n-particle transport code, version 5. Manual